ACSS2 promotes systemic fat storage and utilization through selective regulation of genes involved in lipid metabolism

Zhiguang Huang[a], Menglu Zhang[a], Abigail A. Plec[a], Sandi Jo Estill[a], Ling Cai[b,c], Joyce J. Repa[d], Steven L. McKnight[a,1], and Benjamin P. Tu[a,1]

[a]Department of Biochemistry, University of Texas Southwestern Medical Center, Dallas, TX 75390; [b]Department of Clinical Sciences, University of Texas Southwestern Medical Center, Dallas, TX 75390; [c]Children's Medical Center Research Institute, University of Texas Southwestern Medical Center, Dallas, TX 75390; and [d]Department of Physiology, University of Texas Southwestern Medical Center, Dallas, TX 75390

Contributed by Steven L. McKnight, August 8, 2018 (sent for review April 30, 2018; reviewed by Matthew D. Hirschey, Jared Rutter, and Kathryn E. Wellen)

Acetyl-CoA synthetase 2 (ACSS2) is a conserved nucleocytosolic enzyme that converts acetate to acetyl-CoA. Adult mice lacking ACSS2 appear phenotypically normal but exhibit reduced tumor burdens in mouse models of liver cancer. The normal physiological functions of this alternate pathway of acetyl-CoA synthesis remain unclear, however. Here, we reveal that mice lacking ACSS2 exhibit a significant reduction in body weight and hepatic steatosis in a diet-induced obesity model. ACSS2 deficiency reduces dietary lipid absorption by the intestine and also perturbs repartitioning and utilization of triglycerides from adipose tissue to the liver due to lowered expression of lipid transporters and fatty acid oxidation genes. In this manner, ACSS2 promotes the systemic storage or metabolism of fat according to the fed or fasted state through the selective regulation of genes involved in lipid metabolism. Thus, targeting ACSS2 may offer a therapeutic benefit for the treatment of fatty liver disease.

acetate | epigenetics | fatty liver disease | obesity | metabolism

Acetyl-CoA lies at the nexus of many pathways in central carbon metabolism (1). It is a key intermediate in the catabolism of carbohydrates and fats, which in turn fuels the mitochondrial TCA cycle. In parallel, it also serves as a two-carbon donor for the biosynthesis of fatty acids and sterols, which occurs in the cytosol.

Two primary pathways are involved in the generation of cytosolic acetyl-CoA. One of these pathways is mediated by the ATP citrate lyase enzyme (ACLY) (2), which converts citrate exported from the mitochondria into acetyl-CoA for lipogenesis. Genetic deletion of ACLY in mice results in embryonic lethality (3), suggesting the importance of this pathway as a primary generator of cytosolic acetyl-CoA.

A second pathway is contributed by the acetyl-CoA synthetase (ACS) family of enzymes (4, 5), which are evolutionarily conserved from bacteria to mammals. Knockout mice lacking ACSS2, the nucleocytosolic ACS, are viable and fertile (6), consistent with the idea that it represents an alternative, nonessential pathway for cytosolic acetyl-CoA synthesis. Indeed, acetate, a common product of microbial fermentative metabolism, is not considered a major contributor to mammalian carbon metabolism due to its low concentrations in serum (7). However, mice lacking ACSS2 develop fewer tumors in two mouse models of hepatocellular carcinoma (6), and many tumors are [^{11}C]acetate PET-positive (8), suggesting that the enzyme may supply a critical source of acetyl-CoA under specific conditions. Interestingly, substantial amounts of the enzyme are present in the nucleus (6, 9), hinting that ACSS2 may play a role in the recapture of free acetate released from histone deacetylation (6).

In this study, we sought to further understand the role of acetate and ACSS2 in normal physiology and metabolism. Mammalian *Acss2* was first cloned as a target of the SREBP transcription factors that regulate lipid homeostasis (10). By exposing mice to a high-fat diet (HFD) or prolonged fasting, we found that this simple metabolic enzyme promotes the proper storage or utilization of fat according to the fed or fasted state. As such, ACSS2 has an unanticipated function in the control of systemic lipid metabolism through selective modulation of gene expression linked to acetate availability.

Results

***Acss2* Deletion Protects Against Lipid Deposition and Obesity.** To gain insight into the normal physiological function of ACSS2, we compared *Acss2*-null mice with $Acss2^{+/+}$ and $Acss2^{+/-}$ littermates fed an HFD (58.4% kcal from fat) or a standard diet (chow; 12% kcal from fat) starting at 9 wk of age. The mice on the chow diet exhibited no significant difference in body weight between genotypes over a period of approximately 12 wk. In the mice on the HFD, body weights were significantly lower in both male and female $Acss2^{-/-}$ mice compared with $Acss2^{+/-}$ or $Acss2^{+/+}$ mice (Fig. 1 *A* and *B* and *SI Appendix*, Fig. S1 *A* and *B*). The reduced weight gain observed in $Acss2^{-/-}$ mice was not due to reduced food consumption (*SI Appendix*, Fig. S1 *C* and *D*).

Under HFD conditions, the epididymal fat pads (epWAT) of $Acss2^{-/-}$ mice were notably smaller than those of $Acss2^{+/+}$ mice (*SI Appendix*, Fig. S2*A*). Epididymal fat mass was also significantly

Significance

Animals lacking the ACSS2 enzyme are phenotypically normal when fed a standard chow diet. Surprisingly, when fed a high-fat diet, ACSS2-deficient animals become markedly less obese than their wild-type littermates. We further observe attenuation in the accumulation of fat in the livers of ACSS2-deficient mice. We show that the ACSS2 enzyme acts more like a transcription factor than a metabolic enzyme. It facilitates the dynamic reprogramming of gene expression in many different tissues to orchestrate the proper physiological adaptation of animals to the fed or fasted state. A potent and selective chemical inhibitor of the ACSS2 enzyme could represent a unique therapy for the treatment of both obesity and fatty liver disease.

Author contributions: Z.H., J.J.R., S.L.M., and B.P.T. designed research; Z.H., M.Z., A.A.P., and S.J.E. performed research; Z.H., M.Z., A.A.P., S.J.E., L.C., J.J.R., and B.P.T. analyzed data; and Z.H., S.L.M., and B.P.T. wrote the paper.

Reviewers: M.D.H., Duke University; J.R., University of Utah; and K.E.W., University of Pennsylvania.

The authors declare no conflict of interest.

Data deposition: The data reported in this paper have been deposited in the Gene Expression Omnibus (GEO) database, https://www.ncbi.nlm.nih.gov/geo (accession no. GSE118552).

[1]To whom correspondence may be addressed. Email: steven.mcknight@utsouthwestern.edu or benjamin.tu@utsouthwestern.edu.

This article contains supporting information online at www.pnas.org/lookup/suppl/doi:10.1073/pnas.1806635115/-/DCSupplemental.

Published online September 18, 2018.

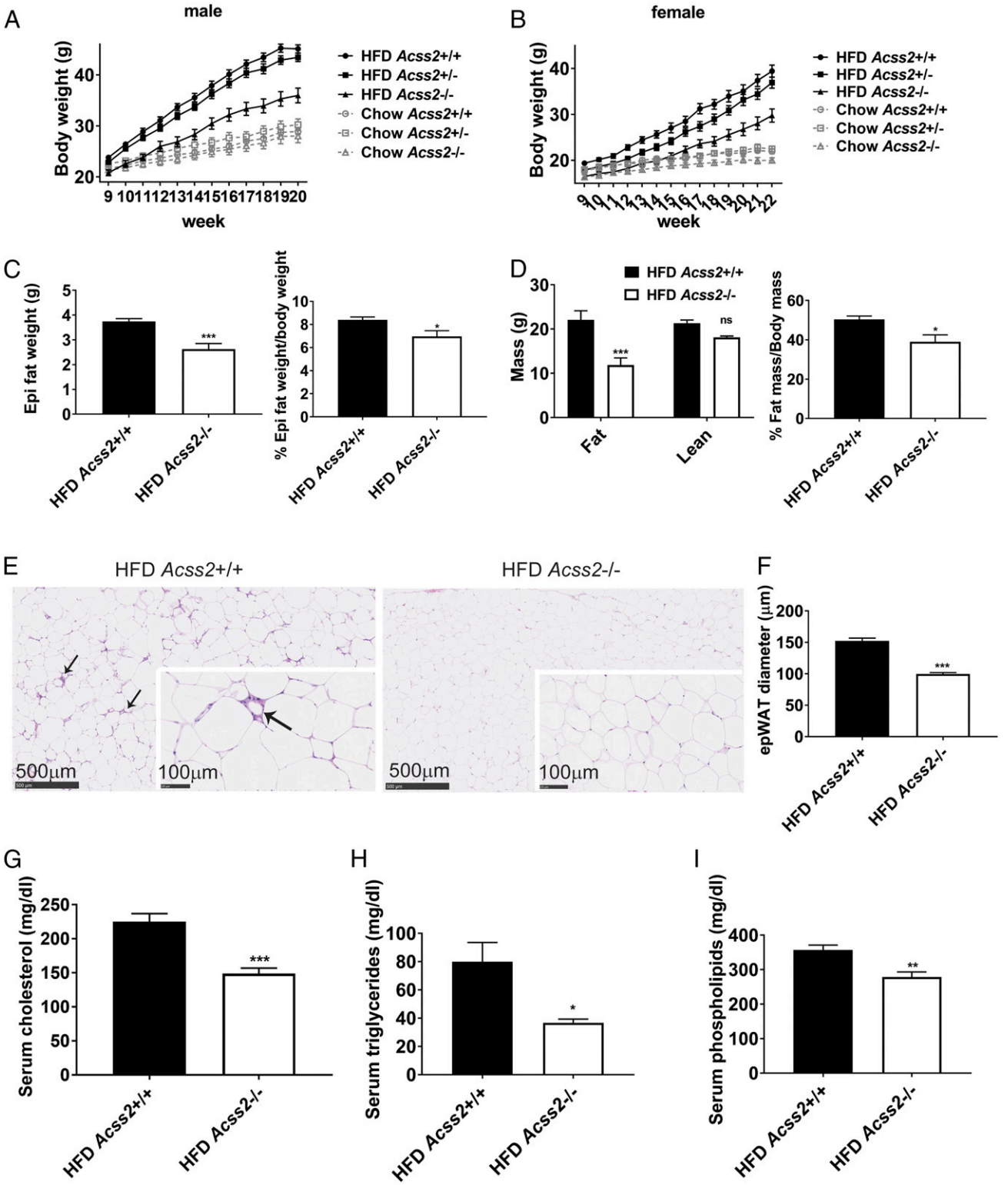

Fig. 1. Effects of *Acss2* deletion on diet-induced obesity. (*A* and *B*) Male (*A*) and female (*B*) $Acss2^{+/+}$, $Acss2^{+/-}$, and $Acss2^{-/-}$ mice were fed chow or an HFD starting at age 9 wk. Body weight was measured weekly (HFD: male $Acss2^{+/+}$, $n = 17$; $Acss2^{+/-}$, $n = 24$; $Acss2^{-/-}$, $n = 14$; female $Acss2^{+/+}$, $n = 15$; $Acss2^{+/-}$, $n = 20$; $Acss2^{-/-}$, $n = 11$; chow diet: male $Acss2^{+/+}$, $n = 10$; $Acss2^{+/-}$, $n = 11$; $Acss2^{-/-}$, $n = 8$; female $Acss2^{+/+}$, $n = 9$; $Acss2^{+/-}$, $n = 13$; $Acss2^{-/-}$, $n = 9$). (*C*) Weight of the epididymal fat depot in $Acss2^{+/+}$ ($n = 14$) and $Acss2^{-/-}$ ($n = 11$) male mice fed an HFD, normalized to body weight. (*D*) Body composition as measured by NMR in $Acss2^{+/+}$ and $Acss2^{-/-}$ male mice ($n = 5$) fed an HFD, normalized to body weight. (*E*) H&E staining of epWAT from male $Acss2^{+/+}$ and $Acss2^{-/-}$ mice fed an HFD ($n = 3$). Arrows denote inflammatory cells. (Scale bars: 500 μm and 100 μm.) (*F*) Diameters of 60 epWAT cells from male $Acss2^{+/+}$ and $Acss2^{-/-}$ mice fed an HFD ($n = 3$). (*G–I*) Levels of serum cholesterol ($n = 10$) (*G*), TG ($n = 7$) (*H*), and phospholipids ($n = 10$) (*I*) in $Acss2^{+/+}$ and $Acss2^{-/-}$ male mice fed an HFD. All data are mean ± SEM. $^{*}P < 0.05$; $^{**}P < 0.01$; $^{***}P < 0.001$.

lower in *Acss2*$^{-/-}$ mice (Fig. 1*C*). NMR assessment of body composition further confirmed reduced total lipid content in *Acss2*$^{-/-}$ mice (Fig. 1*D*). Adipocytes in epWAT of *Acss2*$^{-/-}$ mice showed a reduced size (Fig. 1 *E* and *F*) and decreased inflammatory infiltrates, as well as reduced expression of inflammatory genes (Fig. 1*E* and *SI Appendix*, Fig. S2*B*). Epididymal fat mass, body fat composition, epWAT size, and inflammatory infiltration were not significantly different between *Acss2*$^{+/+}$ and *Acss2*$^{-/-}$ mice fed a chow diet (*SI Appendix*, Fig. S2 *C–F*). Serum cholesterol, triglyceride, and phospholipid concentrations were each significantly decreased in *Acss2*$^{-/-}$ mice fed an HFD (Fig. 1 *G–I*), while no significant differences were observed in *Acss2*$^{-/-}$ mice fed a chow diet (*SI Appendix*, Fig. S3 *A–C*). Taken together, these results indicate that the absence of ACSS2 impedes fat deposition and obesity associated with high dietary-fat intake.

***Acss2* Deletion Protects Against Hepatic Steatosis.** Insulin resistance and hepatic steatosis are two common pathological phenotypes associated with obesity. Under HFD conditions, we observed no significant differences in the levels of serum glucose and insulin between *Acss2*$^{+/+}$ and *Acss2*$^{-/-}$ mice (*SI Appendix*, Fig. S4); moreover, similar glucose clearance and insulin sensitivity were observed in *Acss2*$^{+/+}$ and *Acss2*$^{-/-}$ mice (*SI Appendix*, Fig. S5). These results suggest that although ACSS2 deficiency might protect against obesity, it does not protect against the development of insulin resistance.

The majority of *Acss2*$^{+/+}$ animals developed moderate to severe hepatic steatosis under HFD conditions. Hepatic steatosis was significantly decreased in the majority of *Acss2*$^{-/-}$ mice fed an HFD (Fig. 2*A* and *SI Appendix*, Fig. S6). Liver mass and liver TG accumulation were accordingly decreased in *Acss2*$^{-/-}$ mice (Fig. 2 *B* and *C*). Under chow diet conditions, *Acss2*$^{-/-}$ livers were comparable to *Acss2*$^{+/+}$ livers in morphology and mass (*SI Appendix*, Fig. S7 *A* and *B*). We analyzed livers for expression of a panel of genes involved in lipid metabolism (Fig. 2 *D–G*). The absence of ACSS2 was associated with decreased expression of "master" transcriptional regulators of lipid metabolism (*Ppara*, *pparg*, and *Srebp1c*), as well as key genes involved in fatty acid uptake and trafficking (*Cd36*, *Fatp4*, *Fabp1*, and *Fabp2*), lipid synthesis (*Fas*, *Scd1*, *Hcs*, *Hcr*, *Dhcr24*, *Lss*, and *Gpat1*), and peroxisomal fatty acid oxidation (*Acox1*, *Ehhadh*, *Dbp*, *Acaa1*, and *Scp2*). Reduced expression of these lipid metabolism genes likely accounts for decreased levels of TG and lipids in circulation and in the liver. On the chow diet, there was no significant difference in the expression of genes involved in fatty acid uptake and transport between *Acss2*$^{+/+}$ and *Acss2*$^{-/-}$ livers (*SI Appendix*, Fig. S7*C*).

***Acss2* Deletion Reduces Intestinal Lipid Absorption.** We next evaluated intestinal lipid absorption as a possible mechanism for the reduced weight gain and hepatic steatosis seen in *Acss2*$^{-/-}$ mice. Under HFD conditions, the length of the small intestine was shorter in *Acss2*$^{-/-}$ mice compared with *Acss2*$^{+/+}$ mice (Fig. 3*A*). Although crypt number did not differ among genotypes, *Acss2*$^{-/-}$ mice exhibited slightly shorter villi (*SI Appendix*, Fig. S8). Fecal lipid content was increased by approximately 25% in *Acss2*$^{-/-}$ mice fed an HFD (Fig. 3*B*), but the HFD was not associated with a change in stool color, consistency, output, or daily dietary lipid intake (*SI Appendix*, Fig. S9*A*). In the fed condition on the HFD, fewer and smaller lipid droplets were observed in the mucosa of the proximal intestine of *Acss2*$^{-/-}$ mice (*SI Appendix*, Fig. S9*B*).

To investigate whether the reduction of lipid droplets in the intestine was due to reduction of lipid absorption, we fasted the mice overnight and subjected them to olive oil gavage. Consistently, fewer and smaller lipid droplets were noted in the mucosa of the proximal intestine of *Acss2*$^{-/-}$ mice after olive oil gavage compared with *Acss2*$^{+/+}$ mice (Fig. 3*C*).

Lipid absorption in the intestine is controlled by processes of fatty acid uptake and trafficking, TG synthesis, droplet dynamics, chylomicron assembly, and secretion (11). We evaluated mRNA expression in panels of genes in each of these processes in the small intestine as a function of *Acss2* genotype. Notably, FABP1, a major protein responsible for dietary lipid uptake (12), and DGAT1 and DGAT2, principal enzymes in TG synthesis (13), exhibited significantly reduced expression in the intestines of *Acss2*$^{-/-}$ mice (Fig. 3 *D* and *E*). Genes involved in droplet dynamics and chylomicron assembly and secretion did not show significant differences as a function of genotype (*SI Appendix*, Fig. S10). In the mice on a chow diet, no difference in the expression of genes involved in dietary lipid uptake was observed between *Acss2*$^{+/+}$ and *Acss2*$^{-/-}$ small intestines (*SI Appendix*, Fig. S11). We confirmed by immunohistochemical staining that FABP1 protein levels were also reduced in the enterocytes of *Acss2*$^{-/-}$ mice (Fig. 3*F*).

We next examined the distribution of ACSS2 protein in intestinal enterocytes and cells of the intestinal crypt. ACSS2 was present in both nucleus and cytoplasm in the intestinal crypt. In contrast, in the enterocytes, ACSS2 was present predominantly in the nucleus (Fig. 3*G*). Notably, nuclear expression of ACSS2 in enterocytes was reduced in the chow diet and in fasting conditions compared with the HFD condition (Fig. 3*G*). High nuclear ACSS2 protein abundance in enterocytes was correlated with increased expression of FABP1 and lipid absorption genes in HFD-fed mice. These data suggest that ACSS2 expression in enterocytes may reflect dietary-fat intake to regulate the expression of genes involved in intestinal fat absorption and processing.

***Acss2* Deletion Perturbs Lipid Utilization During Prolonged Fasting.** We next investigated the role of ACSS2 following prolonged fasting (48 h). Fasted *Acss2*$^{-/-}$ mice were noticeably weaker and had reduced locomotor activity compared with the *Acss2*$^{+/+}$ mice (data not shown). *Acss2*$^{-/-}$ mice also lost significantly more body weight (Fig. 4*A*), apparently due to increased loss of fat mass compared with lean mass (Fig. 4*B*). Epididymal fat mass levels were also significantly lower in *Acss2*$^{-/-}$ mice following fasting (Fig. 4*C*).

We further analyzed several metabolic parameters in serum as a function of fasting. Glucose levels were significantly lower in *Acss2*$^{-/-}$ mice compared with *Acss2*$^{+/+}$ mice after fasting (Fig. 4*D*). Consistent with the substantial reduction in adipose, nonesterified fatty acid concentrations were significantly higher in *Acss2*$^{-/-}$ mice compared with *Acss2*$^{+/+}$ littermates (Fig. 4*E*), further suggesting a defect in fatty acid uptake in *Acss2*$^{-/-}$ mice. Serum ketone bodies (Fig. 4*F*) were reduced in *Acss2*$^{-/-}$ mice after fasting, indicating that the mobilization and utilization of fatty acids in *Acss2*$^{-/-}$ livers might be perturbed. Consistent with these phenotypes, *Acss2*$^{-/-}$ livers exhibited reduced expression of a panel of genes regulating fatty acid transport and oxidation following fasting (Fig. 4*G*), while expression of fatty acid transport genes was not significantly different on the chow diet (*SI Appendix*, Fig. S7*C*). Interestingly, serum acetate levels did not appear to be elevated in *Acss2*$^{-/-}$ mice during fasting (*SI Appendix*, Fig. S12). On the chow diet, there was no significant differences in resting glucose, serum nonesterified fatty acids (NEFAs), ketone bodies, or acetate levels between *Acss2*$^{+/+}$ and *Acss2*$^{-/-}$ mice (*SI Appendix*, Figs. S3 *D–F* and S12).

We then performed a global analysis of gene expression in *Acss2*$^{+/+}$ and *Acss2*$^{-/-}$ mice livers after a 48-h fast. Pathway analysis revealed that the LXR/RXR pathway was significantly affected (Fig. 4*H*). LXR/RXR are transcription factors regulating lipid homeostasis in such processes as cholesterol metabolism, cholesterol biosynthesis, cholesterol transport, lipoprotein synthesis, lipogenesis, and cholesterol efflux. Multiple genes downstream of LXR/RXR controlling these processes were all down-regulated in *Acss2*$^{-/-}$ livers (Fig. 4*I*). These results suggest

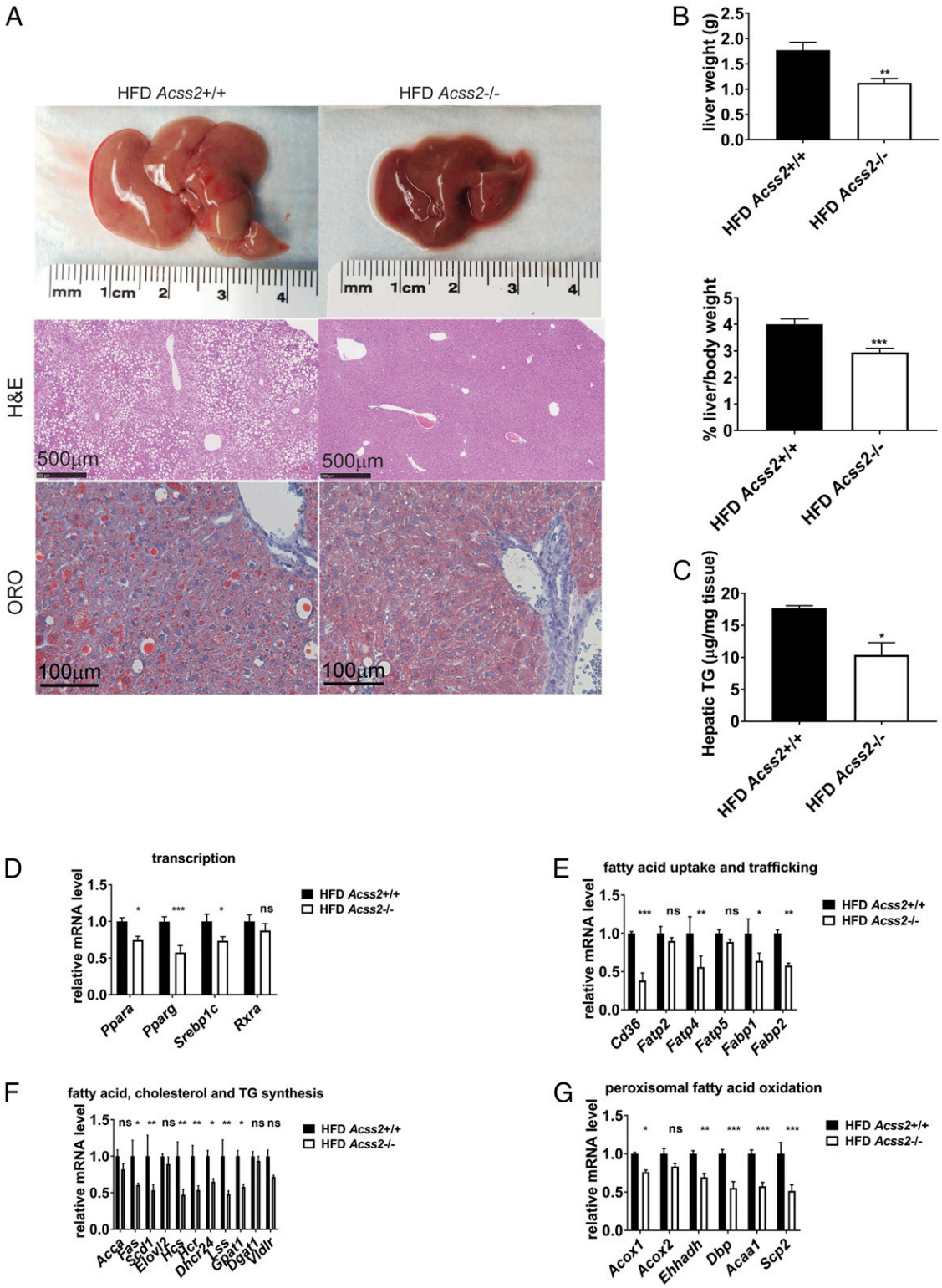

Fig. 2. Effects of *Acss2* deletion on hepatic steatosis in mice fed an HFD. (*A*) General liver appearance, H&E, and ORO imaging from representative male mice fed an HFD for 12 wk starting at age 9 wk. (Scale bar: 500 μm.) See also *SI Appendix*, Fig. S6. (*B*) Mass of livers from $Acss2^{+/+}$ and $Acss2^{-/-}$ male mice fed an HFD for 12 wk ($n = 15$), normalized to body weight. Data are mean ± SEM. $^{**}P < 0.005$. (*C*) Hepatic TG of male mice fed an HFD for 12 wk ($n = 5$). Data are mean ± SEM. $^{*}P < 0.05$. (*D*–*G*) Hepatic mRNA levels in male mice fed an HFD for 12 wk ($n = 4$). Data are mean ± SEM. ns, not significant; $^{*}P < 0.05$; $^{**}P < 0.01$.

that the activity of ACSS2 impacts the expression and activation of LXR/RXR to affect fatty acid and sterol metabolism during prolonged fasting. Therefore, ACSS2 may be required for these transcription factors to optimally express their target genes.

Discussion

In this study, we found that the acetyl-CoA synthetase enzyme ACSS2 regulates a coordinated, systemic response to impact lipid metabolism in the extremes of energy intake (high-fat feeding or

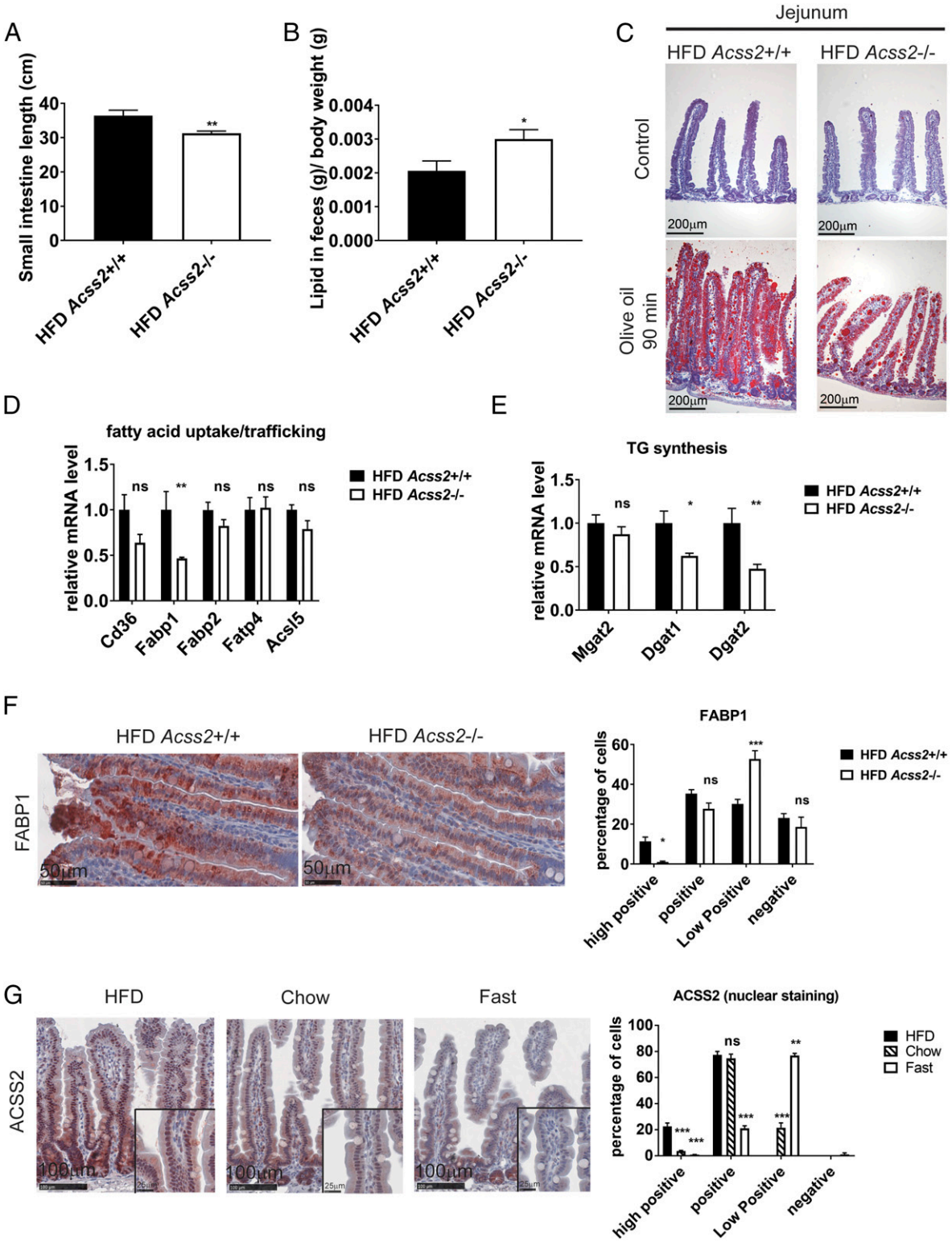

Fig. 3. *Acss2* deletion reduces intestinal lipid absorption. (*A*) The average lengths of small intestines of $Acss2^{+/+}$ and $Acss2^{-/-}$ male mice fed an HFD for 12 wk starting at age 9 wk ($n = 15$). Data are mean ± SEM. $^{**}P < 0.01$. (*B*) Fecal lipid content from male mice fed an HFD for 12 wk ($n = 6$) was analyzed. $^{*}P < 0.05$; ns, not significant. (*C*) ORO staining of proximal intestines from representative male mice fed an HFD for 12 wk with or without olive oil by oral gavage after overnight fasting. (Scale bar: 200 μm.) (*D* and *E*) Intestinal mRNA profile of male mice fed an HFD for 12 wk ($n = 4$). Data are mean ± SEM. ns, not significant; $^{*}P < 0.05$; $^{**}P < 0.01$. (*F*) FABP1 immunohistochemical staining of proximal small intestine from $Acss2^{+/+}$ and $Acss2^{-/-}$ male mice fed an HFD for 12 wk. (Scale bar: 50 μm.) Quantitative evaluation and automated scoring of FABP1 expression was analyzed by IHC Profiler (24). (*G*) IHC staining of ACSS2 protein expression in proximal intestines from male mice fed an HFD or chow diet for 12 wk or fasted for 48 h. (Scale bar: 100 μm.) (*Insets*) Higher magnification images of the outlined boxes. Quantitative evaluation and automated scoring of nuclear ACSS2 expression were performed with IHC Profiler (24).

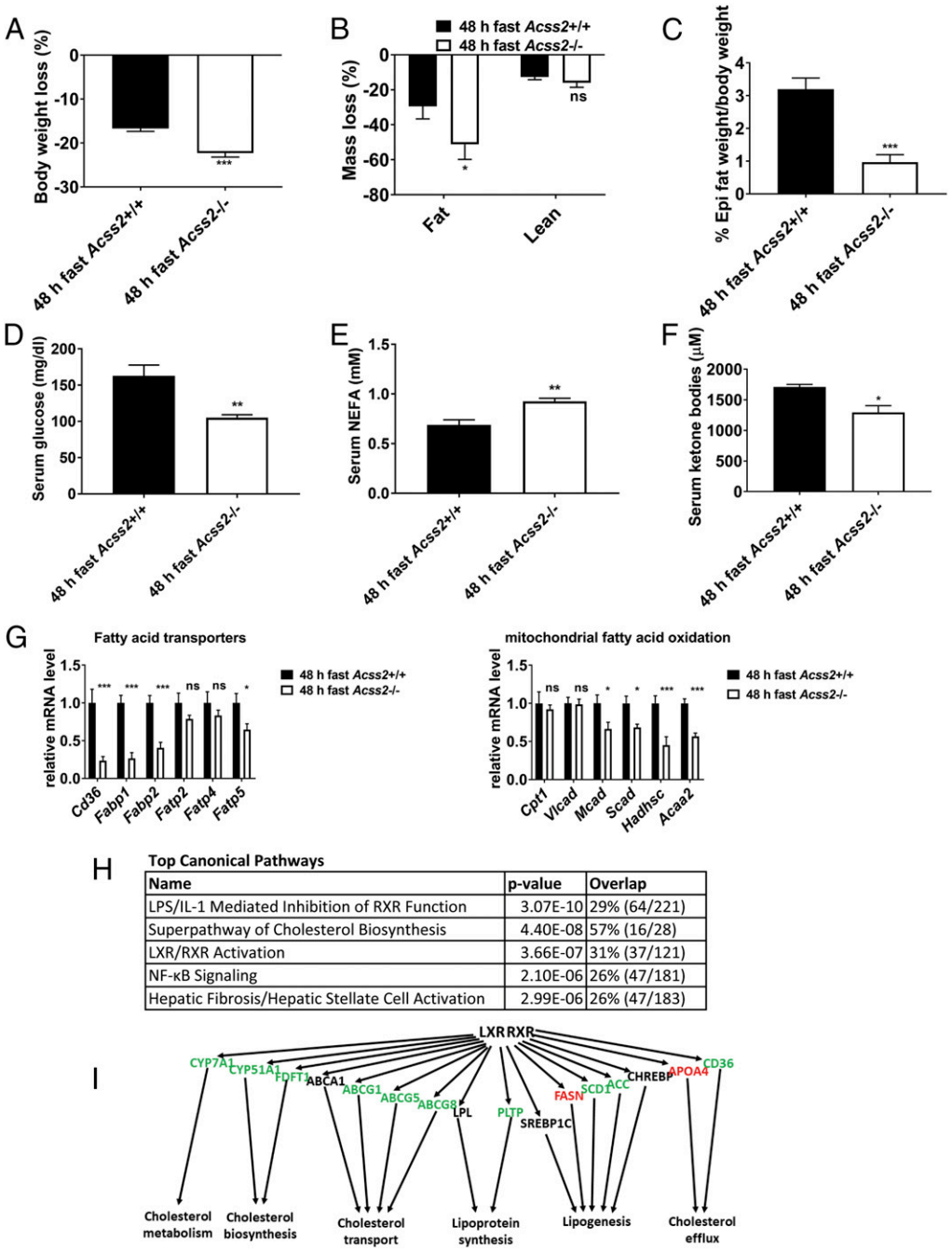

Name	p-value	Overlap
LPS/IL-1 Mediated Inhibition of RXR Function	3.07E-10	29% (64/221)
Superpathway of Cholesterol Biosynthesis	4.40E-08	57% (16/28)
LXR/RXR Activation	3.66E-07	31% (37/121)
NF-κB Signaling	2.10E-06	26% (47/181)
Hepatic Fibrosis/Hepatic Stellate Cell Activation	2.99E-06	26% (47/183)

Fig. 4. *Acss2* deletion perturbs repartitioning of TG from adipose tissue to the liver. (*A*) Percentage reduction in body weight of $Acss2^{+/+}$ ($n = 10$) and $Acss2^{-/-}$ ($n = 8$) male mice after a 48-h fast. Mice were on a chow diet before fasting. (*B*) Percent reductions in fat and lean mass in $Acss2^{+/+}$ and $Acss2^{-/-}$ male mice ($n = 3$) after a 48-h fast. (*C*) Weight of the epididymal fat depot in $Acss2^{+/+}$ ($n = 10$) and $Acss2^{-/-}$ ($n = 8$) male mice measured after a 48-h fast and normalized to body weight. (*D* and *E*) Serum glucose (*D*) and nonesterified fatty acid (*E*) concentrations in $Acss2^{+/+}$ ($n = 10$) and $Acss2^{-/-}$ ($n = 8$) male mice after a 48-h fast. (*F*) Serum ketone body concentrations in $Acss2^{+/+}$ ($n = 10$) and $Acss2^{-/-}$ ($n = 8$) male mice after a 48-h fast. (*G*) Hepatic mRNA profile of $Acss2^{+/+}$ and $Acss2^{-/-}$ male mice after a 48-h fast ($n = 5$). All data are mean ± SEM. ns, not significant; $^*P < 0.05$; $^{**}P < 0.01$. (*H*) RNA-seq performed with hepatic mRNA from $Acss2^{+/+}$ and $Acss2^{-/-}$ male mice after a 48-h fast ($n = 3$). The most affected pathways are indicated. (*I*) Genes with increased expression (red), decreased expression (green), and no change (black) in $Acss2^{-/-}$ livers, segregated by function using IPA Pathway analysis.

prolonged fasting). During fasting, the exaggerated loss of adipose mass in $Acss2^{-/-}$ mice indicates the capacity to hydrolyze TG in adipocytes. However, the concomitant accumulation of NEFA in blood (Fig. 4*E*) suggests inefficiency of fatty acid clearance, uptake, and utilization, which is consistent with decreased expression of major fatty acid transport genes such as *Cd36* and *Fabp1* in $Acss2^{-/-}$ livers (Fig. 4*G*). A decrease in hepatic fatty acid utilization by oxidation is further exemplified by the reduction in serum ketone body concentration, coincident with reduced expression of genes for mitochondrial fatty acid oxidation (Fig. 4*G*). All these observations suggest that the repartitioning of TG energy from adipose tissue to the liver is perturbed in $Acss2^{-/-}$ mice, strongly suggesting that a major function of this enzyme is to promote proper acquisition of energy from fat for organism survival.

Under exposure to an HFD, a consequence of this lipid-dedicated function of ACSS2 is that it then promotes adipose accumulation and hepatic steatosis. Loss of ACSS2 under HFD conditions leads to reduced expression of liver fatty acid transporters, such as CD36 and FABP1 (Fig. 2*E*). Moreover, fatty acid transporters are also down-regulated in *Acss2*$^{-/-}$ enterocytes (Fig. 3 *D–F*), leading to less dietary lipid absorption (Fig. 3*C*) and more lipid in the feces (Fig. 3*B*), which further contribute to lowered serum lipid content (Fig. 1 *G–I*). The correlation between nuclear expression of ACSS2 in enterocytes and the fed state (Fig. 3*G*) raises the possibility that the enzyme coordinates the expression of genes involved in fat absorption with dietary-fat content. In response to an HFD, the enzyme would appear to promote optimal fat uptake and storage, leading to increased weight gain, fat stores, and hepatic steatosis.

The basic function of the ACS family of enzymes is to convert acetate and CoA into acetyl-CoA in an ATP-dependent reaction. We make note of a distinction between the roles of mitochondrial and nucleocytosolic ACS enzymes. Knockout mice lacking ACSS1 have been generated and show hypothermia and reduced energy production while in the fasted state (14). These phenotypes are consistent with the idea that the retrieval of mitochondrial acetate mediated by ACSS1 contributes to mitochondrial energetics and thermogenesis especially on starvation or cold shock. In contrast, the phenotypes reported here give evidence that ACSS2 may promote systemic fat utilization and storage through the selective, coordinated regulation of gene expression across multiple tissues. Our studies suggest that accumulation of nuclear acetate reflects the fasted state and fatty acid availability, and that acetate conversion to acetyl-CoA mediated by ACSS2 may represent an important signal that leads to the selective induction of genes in fat utilization, processing, and storage.

As in vitro transcription from chromatin templates isolated from cells was significantly enhanced by histone acetylation (15), the induction of these genes is likely dependent on the subsequent acetylation of histones mediated by local regeneration of nuclear acetyl-CoA. As such, the nuclear presence of the ACSS2 enzyme enables the effects of a local acetate signal to be magnified and broadcast through epigenetic regulation of genes involved in lipid metabolism. We thus speculate that tumors which express ACSS2 may have enhanced capacity to use fats for cell growth or survival (16, 17).

Hepatic steatosis, which is the first and most readily reversible step in NAFLD, arises from an imbalance between hepatic TG acquisition and removal (18). TGs are assembled by coupling three fatty acids to a glycerol backbone via ester bonds. The fatty acids that are responsible for hepatic TG formation come primarily from three sources: (*i*) diet, (*ii*) de novo synthesis, and (*iii*) adipose tissue (18). In this study, we show how ACSS2 deficiency significantly affects all three sources.

We close by considering the perplexing value of the ACSS2 enzyme for both weight gain by animals availed an abundance of metabolic fuel and survival under conditions of starvation. In the former case, it is sensible to consider the enzyme as a helpful conduit in building lipids for storage in adipose tissue and the liver. Less obvious, by contrast, is a logical consideration of how the ACSS2 enzyme might facilitate adaptation to starved conditions? In this regard we are reminded of histones as a depot for acetate storage (6, 19). Studies of yeast cells under fed or starved conditions have given evidence that the yeast ACS enzymes help facilitate, under conditions of fuel abundance, the acetylation of histone tails associated with genes involved in cell growth (20). Under conditions of starvation, these enzymes recapture acetate resulting from histone deacetylation and promote redistribution of this acetate to histone tails associated with genes required for adaptation to starvation (20). Knowing that the half-life of histone-deposited acetate is measured in only minutes (21, 22), it can be understood that ACS enzymes are responsible for the dynamic redistribution of acetate in a manner that directly regulates yeast cell adaptation to hydrocarbon fuel supply.

The experiments described in this report provide evidence that the nucleocytosolic ACSS2 enzyme of mammals may function via this same regulatory logic to adapt animals to either the fed or starved state. Given that *Acss2*-null mice are viable, it is possible to imagine that a selective inhibitor of ACSS2 might represent a therapeutic strategy useful for the control of either fatty liver disease or obesity.

Materials and Methods

Mouse Studies. All experiments involving animals were conducted under the auspices of the University of Texas Southwestern Medical Center's Animal Care and Use Committee. The *Acss2*$^{+/-}$ and *Acss2*$^{-/-}$ mice were generated as described previously (6). For diet-induced obesity studies, 9-wk-old littermate *Acss2*$^{+/+}$, *Acss2*$^{+/-}$, and *Acss2*$^{-/-}$ mice were fed a chow diet (ENVIGO 2016S) or an HFD (ENVIGO TD.03584) for 10–12 wk. For intestinal lipid uptake study, the mice were fasted overnight, orally gavaged with 200 μL of olive oil, and euthanized either before (control) or 90 min after gavage. The intestine was resected from the ligament of Treitz to the ileocecal junction; divided into proximal, middle, and distal segments of equal length; and washed with cold saline. The jejunum segment was processed for frozen sectioning and Oil Red O (ORO) staining using standard protocols. For the fasting study, mice were individually caged and fasted for 48 h, anesthetized with isoflurane, and exsanguinated by cardiac puncture, after which blood and tissue specimens were collected for subsequent studies.

Serum Metabolite Measurements. Serum cholesterol was measured with a Wako Cholesterol E Kit (439-17501). Serum TG level was measured with a Wako L-Type Triglyceride Kit (461-09891). Serum phospholipids level was measured with a Wako Phospholipid C Kit (433-36201). Serum glucose was measured with a Wako Autokit Glucose (439-90901). Serum NEFA was measured with a Wako HR series NEFA Kit (995-34791). Serum ketone bodies was measured with a Wako Total Ketone Bodies Kit (415-73301). Serum insulin was measured with an ultra-sensitive mouse insulin ELISA kit (90080; Crystal Chem). Measurements were performed according to the manufacturer's protocol.

Glucose Tolerance Test. Mice were fasted overnight for 16 h. Glucose at 1.5 g/kg in saline was injected i.p., and a drop of blood was collected from a tail nick. Glucose was measured at 0, 15, 30, 60, and 120 min postinjection using a glucometer (Bayer).

Insulin Tolerance Test. Mice were fasted for 4 h. Insulin (Thermo Fisher Scientific) at 0.8 U/kg in saline was injected i.p., and a drop of blood was collected from a tail nick. Blood glucose was measured at 0, 15, 30, 60, and 120 min postinjection using a glucometer (Bayer).

Histopathology and Immunohistochemistry. Formalin-fixed, paraffin-embedded tissue sections were either stained with H&E for routine histological evaluation or left unstained for immunohistochemistry (IHC) analysis. The IHC protocol was as described previously (6). The antibodies used in the IHC were ACSS2 (3658; Cell Signaling Technology) and FABP1 (HPA028275; Sigma-Aldrich). OCT-embedded frozen tissues sections were stained with ORO according to a standard protocol and also stained with H&E (*SI Appendix*, Fig. S6). Slides were scanned on a NanoZoomer microscopic slide scanner (Hamamatsu Photonics). Images were captured using NDP view software (Hamamatsu Photonics). Some images were obtained with a conventional microscope instead of with the scanner (Figs. 2*A* and 3*C* and *SI Appendix*, Fig. S6*A*).

Body Composition Measurement. Body composition parameters, including fat mass and lean tissue mass, were measured with a Bruker Minispec mq10. In brief, a mouse was placed in an acrylic cylinder (48-mm diameter) and loosely restrained within the cylinder by pushing a plunger to maintain the animal within a length of 20 cm inside the cylinder depending on the size of the animal. The cylinder is then positioned inside the bore of the magnet. Measurements of fat and lean mass were recorded, and the animals were returned to their home cage in 1 min.

Hepatic TG Extraction. For TG extraction, 50 mg of liver tissue was homogenized in 0.5 mL of PBS. Then 0.4 mL homogenate was added into 1.6 mL of chloroform/methanol, 2:1, vol/vol mixture, and mixed completely by vigorous shaking. The suspension was centrifuged at 845 relative centrifugal force for 10 min at room temperature. The lower organic phase was transferred to

clean tubes and air-dried in a chemical hood overnight. The residual liquid was resuspended in 500–2,000 μL of 1% Triton X-100 in absolute ethanol, and TG concentrations were determined using a Wako L-Type Triglyceride Kit (461-09891). TG levels were normalized to tissue mass.

Real-Time PCR Analysis. Total RNA from frozen liver and intestine mucosa was extracted using TRIzol reagent (Invitrogen). cDNA was synthesized from 2 μg of total RNA with a High-Capacity cDNA Reverse-Transcription Kit (Applied Biosystems). Real-time PCR primer sequences are listed *SI Appendix*, Table S1. Each qRT-PCR was analyzed in duplicate and contained in a final volume of 10 μL: 25 ng of cDNA, each primer at 150 nM, and 5 μL of 2× SYBR Green PCR Master Mix (Applied Biosystems). Results were evaluated by the comparative cycle number at threshold method (23) using cyclophilin as the invariant reference gene.

Fecal Lipid Measurement. Mice were individually housed for 15 d. Food intake and body weight were measured every day. Feces were collected every 3 d and then dried, weighed, and ground. One gram of ground feces was dissolved in 40 mL of Folch solution (2:1 chloroform:methanol) overnight. Solution was filtered with #2 filter paper and filled up to 50 mL. Then 20 mL of the solution and 5 mL of glass-distilled water were added to a glass test tube. Solution was shaken vigorously for 1 min and allowed to separate into two phases. Glass scintillation vials were weighted with analytical balance. The lower phase of the solution was transferred to the glass scintillation vials and dried under gentle air. The vials were weighed again using an analytical balance. Calculations were performed to analyze the fecal lipid content in each mouse.

RNA-Seq. Total RNA from frozen livers of three biological replicates was extracted using TRIzol reagent (Invitrogen). Library construction and sequencing were performed by the University of Texas Southwestern Genomics and Microarray Core Facility, and detailed procedures can be found at the following website: https://microarray.swmed.edu/. RNA-seq results were processed by RNA-seq pipeline, and the source code repository can be accessed at https://git.biohpc.swmed.edu/BICF/Astrocyte/rnaseq. Canonical pathways analysis was performed by Ingenuity Pathway Analysis (IPA) (Qiagen). RNA-seq data have been deposited at GEO (accession no. GSE118552).

Data Analysis. Statistical analysis was performed using Prism (GraphPad Software). Experimental values are shown as mean ± SEM. Statistical significance between two groups was determined using the two-tailed Student's *t* test. One-way ANOVA was applied for multigroup comparisons. *P* values <0.05 were considered significant.

ACKNOWLEDGMENTS. We thank S. Comerford and R. Hammer for helpful discussions and J. Horton for generously sharing Acss2 KO mice. This work was supported by National Institutes of Health Grants R01 CA185169 (to B.P.T. and S.L.M.) and R01 DK078592 (to J.J.R.) and Cancer Prevention and Research Institute of Texas Grant RP170699 (to B.P.T. and S.L.M.).

1. Shi L, Tu BP (2015) Acetyl-CoA and the regulation of metabolism: Mechanisms and consequences. *Curr Opin Cell Biol* 33:125–131.
2. Srere PA (1959) The citrate cleavage enzyme, I: Distribution and purification. *J Biol Chem* 234:2544–2547.
3. Beigneux AP, et al. (2004) ATP-citrate lyase deficiency in the mouse. *J Biol Chem* 279: 9557–9564.
4. Jones ME, Lipmann F, Hilz H, Lynen F (1953) On the enzymatic mechanism of coenzyme A acetylation with adenosine triphosphate and acetate. *J Am Chem Soc* 75:3285–3286.
5. Berg P (1956) Acyl adenylates: An enzymatic mechanism of acetate activation. *J Biol Chem* 222:991–1013.
6. Comerford SA, et al. (2014) Acetate dependence of tumors. *Cell* 159:1591–1602.
7. Psychogios N, et al. (2011) The human serum metabolome. *PLoS One* 6:e16957.
8. Grassi I, et al. (2012) The clinical use of PET with (11)C-acetate. *Am J Nucl Med Mol Imaging* 2:33–47.
9. Ariyannur PS, et al. (2010) Nuclear-cytoplasmic localization of acetyl coenzyme a synthetase-1 in the rat brain. *J Comp Neurol* 518:2952–2977.
10. Luong A, Hannah VC, Brown MS, Goldstein JL (2000) Molecular characterization of human acetyl-CoA synthetase, an enzyme regulated by sterol regulatory element-binding proteins. *J Biol Chem* 275:26458–26466.
11. D'Aquila T, Hung YH, Carreiro A, Buhman KK (2016) Recent discoveries on absorption of dietary fat: Presence, synthesis, and metabolism of cytoplasmic lipid droplets within enterocytes. *Biochim Biophys Acta* 1861:730–747.
12. Storch J, Corsico B (2008) The emerging functions and mechanisms of mammalian fatty acid-binding proteins. *Annu Rev Nutr* 28:73–95.
13. Yen CL, Stone SJ, Koliwad S, Harris C, Farese RV, Jr (2008) Thematic review series: Glycerolipids. DGAT enzymes and triacylglycerol biosynthesis. *J Lipid Res* 49:2283–2301.
14. Sakakibara I, et al. (2009) Fasting-induced hypothermia and reduced energy production in mice lacking acetyl-CoA synthetase 2. *Cell Metab* 9:191–202.
15. Nagai S, Davis RE, Mattei PJ, Eagen KP, Kornberg RD (2017) Chromatin potentiates transcription. *Proc Natl Acad Sci USA* 114:1536–1541.
16. Nieman KM, et al. (2011) Adipocytes promote ovarian cancer metastasis and provide energy for rapid tumor growth. *Nat Med* 17:1498–1503.
17. Blücher C, Stadler SC (2017) Obesity and breast cancer: Current insights on the role of fatty acids and lipid metabolism in promoting breast cancer growth and progression. *Front Endocrinol (Lausanne)* 8:293.
18. Cohen JC, Horton JD, Hobbs HH (2011) Human fatty liver disease: Old questions and new insights. *Science* 332:1519–1523.
19. Ye C, Tu BP (2018) Sink into the epigenome: Histones as repositories that influence cellular metabolism. *Trends Endocrinol Metab* 29:626–637.
20. Cai L, Sutter BM, Li B, Tu BP (2011) Acetyl-CoA induces cell growth and proliferation by promoting the acetylation of histones at growth genes. *Mol Cell* 42: 426–437.
21. Jackson V, Shires A, Chalkley R, Granner DK (1975) Studies on highly metabolically active acetylation and phosphorylation of histones. *J Biol Chem* 250:4856–4863.
22. Waterborg JH (2002) Dynamics of histone acetylation in vivo: A function for acetylation turnover? *Biochem Cell Biol* 80:363–378.
23. Schmittgen TD, Livak KJ (2008) Analyzing real-time PCR data by the comparative C(T) method. *Nat Protoc* 3:1101–1108.
24. Varghese F, Bukhari AB, Malhotra R, De A (2014) IHC profiler: An open source plugin for the quantitative evaluation and automated scoring of immunohistochemistry images of human tissue samples. *PLoS One* 9:e96801.